DOI: 10.1002/((please add manuscript number))
Article type: Communication

Labyrinth Metasurface Absorber for Ultra-High-Sensitivity Terahertz Thin Film Sensing

*Irati Jáuregui-López, Pablo Rodríguez-Ulibarri, Aitor Urrutia, Sergei A. Kuznetsov, Miguel Beruete**

I. Jáuregui-López, Dr. P. Rodríguez-Ulibarri, Dr. M. Beruete
Antennas Group-TERALAB
Electric and Electronic Engineering Department
Universidad Pública de Navarra
Campus Arrosadía, 31006 Pamplona, Spain
E-mail: miguel.beruete@unavarra.es

Dr. A. Urrutia, Dr. M. Beruete
Institute of Smart Cities
Public University of Navarra
31006 Pamplona, Spain

Dr. S. A. Kuznetsov
Novosibirsk State University
Pirogova 2, 630090 Novosibirsk, Russia.
Rzhanov Institute of Semiconductor Physics SB RAS
Novosibirsk Branch "TDIAM."
Lavrentiev Ave. 2/1, 630090 Novosibirsk, Russia
E-mail: SAKuznetsov@nsm.nsu.ru

Keywords: metasurfaces, sensing, thin film, terahertz

Abstract: In this work a labyrinth metasurface sensor operating at the low-frequency edge of the THz regime is presented. This intricate shape leads to a high electric field confinement in the surface of the structure, leading to ultrasensitive performance, able to detect samples of the order of tens of nanometers at a wavelength of the order of millimeters (i.e. 4 orders of magnitude larger). The sensing capabilities of the metasurface are evaluated numerically and experimentally by covering the metallic face with tin dioxide (SnO2) thin films with thicknesses ranging from ha = 24 nm, to ha = 345 nm. A redshift of the resonant frequency is observed as the analyte thickness increases, until reaching a thickness of 20 µm, where the response saturates. A maximum sensitivity of more than 800 and a FoM near 4500 are achieved, allowing discriminating differences in

the SnO2 thickness of less than 25 nm, and improving previous works by a factor of 55. This result could open a new paradigm of ultrasensitive devices based on intricate metageometries overcoming the limitations of classical metasurface sensor designs based on periodic metaatoms.

The THz band (from 0.1 to 10 THz) has been historically known as the "THz gap" [1] due to the lack of efficient emitters and receivers operating in this regime at ambient temperature. However a series of recent breakthroughs have helped to bridge this gap, to the extent that nowadays it is a field of intense and multidisciplinary research with many applications coming into reality in numerous sectors, like medicine, security, communications, space, or sensing, among others.[2] Sensing at THz is of special relevance, because many substances exhibit molecular vibrations opening new routes for high performance detection platforms, allowing the detection of certain gases or solids that show absorption lines in this frequency range. Moreover, due to a larger wavelength and deeper penetration into many materials versus the visible or infrared ranges, THz waves are promising for examining optically opaque coatings. To date, several strategies have been followed to develop THz sensing devices such as plasmonic structures,[3] metamaterials,[4] and frequency selective surfaces,[5] among others. One of the biggest open challenges of

THz research is the detection of very thin samples hardly detectable with conventional methods, so called thin films. As explained in[6], thin-film sensing techniques find application in a variety of circumstances: when the amount of sample is very small; when the sample is most easily processed in thin-film form; when a thin-film sample has different properties from its bulk counterpart; when the sensitivity is better using a thin-film; or when the characterization is complementary to some other thin-film technique, such as atomic layer deposition. Different solutions have been proposed, including waveguides, transmission line and waveguide filters, resonators as well as plasmonic structures. Metasurfaces are emerging as a revolutionary alternative thanks to the exciting properties they offer compared to classical sensing techniques and also because the system complexity is reduced compared to

the previous techniques.[6] These artificial structures can be considered as the two-dimensional equivalents of metamaterials and consist of planar screens engineered to have a customized electromagnetic response.[7,8] They are generally designed by assembling arrays of resonators whose size and spacing are much smaller than the operation wavelength and with geometric parameters such as shape, size, etc. that can be modified to create a desired frequency response, giving rise to devices with unconventional performance such as Generalized Snell's Law structures,[8] planar lenses,[7] enhanced spin-Hall effect,[9] wavefront mathematical computation[10] or even optical cloaking.[11,12]

Thin-film sensors based on metasurfaces exploit the strong electric field concentration that appears in gaps of the metallic pattern when the metasurface is at resonance. Therefore, the response of the system is very dependent on the characteristics of the thin film deposited on top. Most of the works to date consist of canonical periodic structures such as split-ring resonators (SRRs) and their modified versions.[6,13–15] There are also examples in the literature that exploit extraordinary transmission[16], periodic slits in a metallic plane[17] or asymmetric SRRs that improve the sensing performance by exciting high Q resonances and hence reducing the spectral linewidth.[18,19]. In addition, it has been demonstrated that absorbers working in reflection are better for sensing purposes than metasurfaces working in transmission.[20,21] Although these examples work well as sensing platforms, they usually suffer from a relatively poor performance achieving small sensitivity values (less than 80 in the best case[14]). Recently, new fabrication techniques have pushed forward the field by allowing the creation of nanogap structures,[22,23] able to achieve values of the sensitivity of the order of 4400[22], at the expense of requiring a relatively complex manufacturing procedure

In this work we demonstrate a so-called labyrinth-shaped THz metasurface absorber for high performance thin-film detection with extreme sensitivity using conventional manufacturing procedures. This way, the complexity is put only in the design, alleviating the fabrication constraints that relies on standard contact photolithography.

Our strategy is based on the convoluted geometry of a labyrinth-shaped micro-pattern that improves the field concentration all along the metasurface and not only at discrete spots, unlike the sensors based on canonical periodic structures. This shift from meta-atoms to more elaborated meta-geometries allows the detection of exceedingly thin dielectric samples deposited on top of the metasurface, with thickness and thickness increments in the nanometre scale at an operation wavelength in the millimetre scale. Hence, the developed sensor is able to discern films as thin as $\sim 10^{-5}\lambda_0$, with λ_0 the free-space operation wavelength. An outstanding sensitivity value of more than 800 with a FoM near 4500 nm is achieved, improving by a factor of 55 previous reports.[20] Although convoluted and Hilbert space-filling surfaces similar to the one studied here have been investigated at microwaves in the past as frequency selective surfaces, artificial magnetic conductors (AMC) and absorbers,[24–26] the use of this kind of structures as ultrasusceptible sensing devices operating at THz frequencies has not been explored yet in the literature.

The unit cell of the labyrinth metasurface absorber with relevant dimensions as well as a microscopic image of the fabricated structure is shown in **Figure 1**(a) and (c) respectively. The metasurface consists of a triangular-lattice array of convoluted-shaped apertures manufactured as a continuous aluminium layer lithographically patterned on a polypropylene (PP) slab with uniform back metallization (i.e. ground plane (GP)). Each elementary aperture is designed as a centre-connected strip element having 120° rotational symmetry. The choice of PP is explained by its small loss tangent value ($\tan\delta \approx 1\times10^{-3}$) in the THz domain that enables enhancing the Q-factor of the metasurface absorber[27] and therefore maximizing the FoM of the metasurface sensor (which is proportional to the Q-value[6]).

Originally, the labyrinth metasurfaces were developed for using without the GP-layer and were intended for filtering applications in diagnostic systems of millimetre-wave radiation generated in schemes with free-electron masing[28,29] and electron-beam-induced emission from hot

magnetized plasmas[30,31]. The metasurface pattern was designed to fix the transmission passband near 75 GHz and achieve at the same time strong suppression around 150 GHz combined with the requirement of maintaining a super-stable spectral characteristic under oblique illumination **(Figure 2)**. As it is known, the angular stability of a resonance in any periodic array improves when the resonance frequency f_{res} occurs far below the onset of the first diffraction order f_{diff}, i.e. when $f_{res} << f_{diff}$. In this regard, triangular lattices outperform square-lattice solutions given that f_{diff} can be $\sqrt{2}/3$ times higher. This is why a metasurface with a triangular unit cell was selected. The actual metasurface dimensions indicated in Figure 1 were chosen from the conditions imposed by our fabrication capabilities (see supporting information) and the aforementioned requirements on the filtering performance of the GP-free metasurface. The underlying design principle for such metasurfaces is based on the fact that the convoluted geometry of the metallic strips and the inter-strip gaps noticeably increases their total length within the metasurface unit cell compared to non-convoluted geometries. From an equivalent circuit perspective[32,33], this factor considerably augments the effective lumped inductance L and capacitance C of the structure and, therefore, induces a much more noticeable red shift of its resonant frequency f_{res} according to the relation $2\pi f_{res} = 1/(LC)^{1/2}$. As a result, a 20-fold reduction of the central frequency of the fundamental transmission passband ($f_{res} \cong 75$ GHz) relative to the onset of the first diffraction order located at $f_{diff} = 1500$ GHz (assuming normal incidence) is achieved, yielding excellent angular stability as shown in Figure 2 (all the simulation results in the paper are obtained with the commercial simulator CST Microwave Studio® following the methodology described in the supporting information). A detailed study of the GP-free metasurface will be presented elsewhere.

Prior to analysing the sensing performance of the labyrinth metasurface in the absorber regime (i.e. after adding the GP-layer), we will analyse first the metasurface absorber without any analyte on top assuming normal incidence and both vertical and horizontal polarizations. As

the ground plane blocks any transmission, we will only consider the reflection coefficient – both copolar and crosspolar components – in the following. We start the study with the lossless case, green curves in **Figure 3**. As shown there, the reflection coefficient magnitude is nearly 1 (solid green) all along the spectrum, except at $f \cong 137.6$ GHz where a small cross-polarization peak appears (dashed green). When losses are considered, a sharp resonance dip appears at $f_0 = 135.3$ GHz (solid blue curve). The dip is caused by energy dissipation in the metasurface (which occurs mainly in the convoluted metallization, see supporting information) and not by cross-polarization of the reflected wave, as demonstrated by the low magnitude (less than –49 dB) of the crosspolar reflection coefficient magnitude (dashed blue curve). It is to be noticed that the absorption resonance is positioned near the band-stop transmission resonance of the GP-free metasurface, i.e. almost doubly exceeding the central frequency of 75 GHz of its fundamental passband (Figure 2). This is explained by the fact that the near-unity absorptivity for any metasurface absorber patterned on an electrically thin GP-backed dielectric layer can be attained only at frequencies where the impedance of the patterned layer is capacitive.[27,34] Unlike the conventional meta-absorbers with electrically isolated metallic elements (e.g. patches) forming the top patterned layer whose low-frequency impedance is always capacitive, the labyrinth pattern considered here is comprised by electrically connected convoluted metallic stripes whose impedance at low frequencies is fundamentally inductive. The capacitive component in the stripes' impedance, however, becomes dominant over the inductive one above the passband (but below the stopband resonance) that allows fulfilling the absorber criterion. Furthermore, as shown in the supporting information, the response is independent of the wave polarization (the same happened for the lossless case) which is an enormous advantage for sensing purposes. Therefore, we will hereafter assume only vertical polarization in the rest of the calculations without loss of generality.

The sensing capability of the metasurface was evaluated by coating the labyrinth face with tin dioxide (SnO_2) thin films, whose permittivity is $\varepsilon_a \approx 4$ at the operation wavelength.[35,36] The SnO_2 coatings were prepared by the sputter-deposition technique[37]. The experimental characterization was carried out with an ABmm™ Vector Network Analyser (VNA) MVNA-8-350-4 equipped with a quasioptical bench working in the reflection configuration. More information about the samples preparation and experimental methodology can be found in the supplementary information.

In **Figure 4** is plotted the absorbance for several thicknesses of the SnO_2 film: h_a = 24 nm ($1.1\times10^{-5}\lambda_0$); 58 nm ($2.6\times10^{-5}\lambda_0$); 108 nm ($4.9\times10^{-5}\lambda_0$); 345 nm ($15.6\times10^{-5}\lambda_0$), numerical simulations in panel (a) and experimental measurements in panel (b). From these results we can obtain the wavelength shift as the analyte thickness is varied, displayed in panel (c). It is noteworthy the extreme sensitivity of the labyrinth structure, able to discriminate differences in SnO_2 thickness of less than 25 nm even for a relatively low dielectric constant. In terms of the operation wavelength this means that the sensor is able to detect variations of only ~$1.1\times10^{-5}\lambda_0$, very much beyond the state-of-the-art sensing platforms which achieve, in the best case[14], a value around $1.7\times10^{-4}\lambda_0$. This is even more remarkable if one notices that the analyte does not fill completely the groove between metal strips, as sketched in Figure 1(b). We performed an additional simulation study increasing the analyte thickness and found that the response saturates when the thickness is nearly 20 μm ($0.009\lambda_0$) whereas for ultrathin analytes (h_a < 10 μm) the response is approximately linear. As a side comment, we can observe in the experimental curve of the sample with h_a = 345 nm a small dip arising at 147.5 GHz.

We can quantify the performance of the sensor more formally by calculating its sensitivity (S) and FoM. One can find in the literature different definitions of the sensitivity in the context of thin-film sensing, see[14,15,20]. Arguably, the most universally accepted definition relates the variation of the resonance wavelength with the variation of the analyte thickness: $S = \Delta\lambda/h_a$

where $\Delta\lambda = \lambda_a - \lambda_0$ with λ_a the resonance wavelength at each h_a and λ_0 the resonance wavelength without the analyte. Note that in refractometer applications the variation of the refractive index is also included but in our case we do not need to do this, as our aim is to detect only thickness variations. For the sake of completeness, a detailed comparative study of the sensor performance with other works in the literature using other sensitivity definitions is presented in the supplementary information. The FoM is a more refined parameter to assess the quality of a sensor and is defined as the ratio between the sensitivity and the full width at half minimum (FWHM) in wavelength dimensions: FoM = S/FWHM. A high FoM ensures a good resonance shift with analyte variation along with a narrow spectral line, avoiding overlap between different curves.

The values of the Sensitivity and FoM for the designed structure are presented in **Table 1**, along with the values obtained for a new sample with the same fabrication parameters, but different analyte thicknesses, presented in **Table 2** (results shown in the supplementary information). They reach significantly high values both in simulation and measurement. In the experiment the maximum is obtained for h_a = 108 nm, where the sensitivity is ~578 and the FoM is ~ 3558 nm^{-1}. These values are much higher than those found in the literature with similar fabrication techniques as the method used in this paper, as it can be seen at the comparison of **Table 3** (note that we have different results than the ones presented in the references due to our method to calculate the sensitivity and FoM), where the maximum FoM was ~118 nm^{-1}.

This excellent sensing performance of the labyrinth structure can be explained by its intricate geometry that provokes a strong electrical coupling between adjacent metallic strips. In very subwavelength structures, such as the one considered here, the electric field is strongly confined near the surface, so we can achieve high sensitivity to slight changes of the thickness of the thin-film layer deposited on top. To get a clearer view, we have obtained the electric field distribution of this structure at both sides of the labyrinth. As shown there, the field pattern is

approximately symmetric at both sides of the metallization. Therefore, although there is indeed some field concentration inside the substrate, the field in the air interface is able to interact closely with the analyte. This is corroborated in Figure 4(d) where it is shown that the saturation is reached for an analyte thickness of around 20 μm. Moreover, while in other sensing platforms the electric field starts to vanish at significantly larger distances, in the labyrinth structure the electric field starts to decline at only $5\times10^{-4}\lambda_0$ (corresponding to ~1 μm away from the metasurface outer face), where the magnitude of the electric power decreases to the half (see **Figure 5**). Note that if we use denormalized values for the *x*-axis in panel (b), the value $0.01\lambda_0$, corresponds to 25 μm, which is the thickness where the response starts to saturate (see Figure 4(d)). This highlights the importance of the electric field confinement for sensing purposes.

To conclude, we have reported here a labyrinth metasurface which operates in the near-to-unity absorptivity regime at the low-frequency edge of the THz spectrum and exhibits extreme FoM and sensitivity to thin film detection, exceeding largely the results found in the literature by a factor of 30, if we compare our work with similar structures. Note that recently higher sensitive values can be obtained as shown in[23], but at the expense of more complex designs and fabrication procedures. The performance of the structure has been numerically and experimentally tested with high values of sensitivity that vary between 300 and 800, and a FoM between 2000 nm^{-1} and 4500 nm^{-1}. These extremely high values are explained by the strong electric field confinement achieved by the intricate labyrinth shape. The proposed approach constitutes an important step toward the fabrication of high sensitivity thin film sensors and could be extrapolated towards biosensors able to detect biological samples such as bacteria, proteins, or DNA, among others. It is worth noting that the metasurface sensor investigated in this work operates at relatively long waves ($\lambda_0 \sim 2.2$ mm) that potentially allows one to employ more compact and less expensive field-oriented millimetre-wave instrumentation than it is required for higher-frequency THz spectral measurements. We foresee these results as a proof-

of-concept that could be extended in the future to biological sensing, where thin-film samples become essential.

Supporting Information
Supporting Information is available from the Wiley Online Library or from the author.

Acknowledgements
The authors acknowledge support from the Spanish Ministerio de Economía y Competitividad (MINECO) under Contract TEC2014-51902-C2-2-R and the NSU program 5-100 established by the Russian Ministry of Education and Science.

Received: ((will be filled in by the editorial staff))
Revised: ((will be filled in by the editorial staff))
Published online: ((will be filled in by the editorial staff))

References

[1] M. Tonouchi, *Nat. Photonics* **2007**, *1*, 97.

[2] D. Saeedkia, *Handbook of Terahertz Technology for Imaging, Sensing and Communications*, WP Woodhead Publishing, **2013**.

[3] B. Ng, J. Wu, S. M. Hanham, A. I. Fernández-Domínguez, N. Klein, Y. F. Liew, M. B. H. Breese, M. Hong, S. A. Maier, *Adv. Opt. Mater.* **2013**, *1*, 543.

[4] T. Driscoll, G. O. Andreev, D. N. Basov, S. Palit, S. Y. Cho, N. M. Jokerst, D. R. Smith, *Appl. Phys. Lett.* **2007**, *91*, 062511.

[5] C. Debus, P. H. Bolivar, *Appl. Phys. Lett.* **2007**, *91*, 184102.

[6] J. F. O'Hara, W. Withayachumnankul, I. Al-Naib, *J. Infrared, Millimeter, Terahertz Waves* **2012**, *33*, 245.

[7] A. V. Kildishev, A. Boltasseva, V. M. Shalaev, *Science* **2013**, *339*, 1232009.

[8] N. Yu, F. Capasso, *Nat. Mater.* **2014**, *13*, 139.

[9] X. Yin, Z. Ye, J. Rho, Y. Wang, X. Zhang, *Science* **2013**, *339*, 1405.

[10] A. Silva, F. Monticone, G. Castaldi, V. Galdi, A. Alù, N. Engheta, *Science* **2014**, *343*,

160.

[11] X. Ni, Z. J. Wong, M. Mrejen, Y. Wang, X. Zhang, *Science* **2015**, *349*, 1310.

[12] B. Orazbayev, N. Mohammadi Estakhri, A. Alù, M. Beruete, *Adv. Opt. Mater.* **2017**, *5*, 1600606.

[13] W. Withayachumnankul, H. Lin, K. Serita, C. M. Shah, S. Sriram, M. Bhaskaran, M. Tonouchi, C. Fumeaux, D. Abbott, *Opt. Express* **2012**, *20*, 3345.

[14] H. Tao, A. C. Strikwerda, M. Liu, J. P. Mondia, E. Ekmekci, K. Fan, D. L. Kaplan, W. J. Padilla, X. Zhang, R. D. Averitt, F. G. Omenetto, *Appl. Phys. Lett.* **2010**, *97*, 261909.

[15] C. Sabah, H. G. Roskos, *Microsyst. Technol.* **2012**, *18*, 2071.

[16] L. Xie, W. Gao, J. Shu, Y. Ying, J. Kono, *Sci. Rep.* **2015**, *5*, 8671.

[17] D.-K. Lee, J.-H. Kang, J.-S. Lee, H.-S. Kim, C. Kim, J. Hun Kim, T. Lee, J.-H. Son, Q.-H. Park, M. Seo, *Sci. Rep.* **2015**, *5*, 15459.

[18] R. Singh, W. Cao, I. Al-Naib, L. Cong, W. Withayachumnankul, W. Zhang, *Appl. Phys. Lett.* **2014**, *171101*, 5.

[19] I. A. I. Al-Naib, C. Jansen, M. Koch, *Appl. Phys. Lett.* **2008**, *93*, 083507.

[20] L. Cong, S. Tan, R. Yahiaoui, F. Yan, W. Zhang, R. Singh, *Appl. Phys. Lett.* **2015**, *106*, 031107.

[21] R. Yahiaoui, S. Tan, L. Cong, R. Singh, F. Yan, W. Zhang, *J. Appl. Phys.* **2015**, *118*, 083103.

[22] N. Kim, S. In, D. Lee, J. Rhie, J. Jeong, D. S. Kim, N. Park, *ACS Photonics* **2018**, *5*, 278.

[23] H. R. Park, X. Chen, N. C. Nguyen, J. Peraire, S. H. Oh, *ACS Photonics* **2015**, *2*, 417.

[24] B. Sanz-Izquierdo, E. A. T. Parker, J.-B. Robertson, J. C. Batchelor, *IEEE Trans. Antennas Propag.* **2010**, *58*, 690.

[25] F. Huang, J. C. Batchelor, E. A. Parker, *Electron. Lett.* **2006**, *42*, 788.

[26] J. McVay, A. Hoorfar, N. Engheta, *Microw. Opt. Technol. Lett.* **2009**, *51*, 785.

[27] S. A. Kuznetsov, A. G. Paulish, M. Navarro-Cía, A. V. Arzhannikov, *Sci. Rep.* **2016**, *6*, 21079.

[28] M. A. Agafonov, A. V. Arzhannikov, N. S. Ginzburg, V. G. Ivanenko, P. V. Kalinin, S. A. Kuznetsov, N. Y. Peskov, S. L. Sinitsky, *IEEE Trans. Plasma Sci.* **1998**, *26*, 531.

[29] A. V. Arzhannikov, N. S. Ginzburg, P. V. Kalinin, S. A. Kuznetsov, A. M. Malkin, N. Y. Peskov, A. S. Sergeev, S. L. Sinitsky, V. D. Stepanov, M. Thumm, V. Y. Zaslavsky, *Phys. Rev. Lett.* **2016**, *117*, 114801.

[30] A. V. Burdakov, A. V. Arzhannikov, V. S. Burmasov, I. A. Ivanov, M. V. Ivantsivsky, I. V. Kandaurov, S. A. Kuznetsov, V. V. Kurkuchekov, K. I. Mekler, S. V. Polosatkin, S. S. Popov, V. V. Postupaev, A. F. Rovenskikh, V. F. Sklyarov, M. K. A. Thumm, Y. A. Trunev, L. N. Vyacheslavov, *Fusion Sci. Technol.* **2013**, *63*, 286.

[31] A. V. Arzhannikov, A. V. Burdakov, V. S. Burmasov, D. E. Gavrilenko, I. A. Ivanov, A. A. Kasatov, S. A. Kuznetsov, K. I. Mekler, S. V. Polosatkin, V. V. Postupaev, A. F. Rovenskikh, S. L. Sinitsky, V. F. Sklyarov, L. N. Vyacheslavov, *Phys. Plasmas* **2014**, *21*, 082106.

[32] B. A. Munk, *Frequency Selective Surfaces: Theory and Design*, Wiley-Interscience, **2000**.

[33] F. Costa, A. Monorchio, G. Manara, *Appl. Comput. Electromagn. Soc. J.* **2014**, *29*, 960.

[34] F. Costa, S. Genovesi, A. Monorchio, G. Manara, *IEEE Trans. Antennas Propag.* **2013**, *61*, 1201.

[35] S. Baco, A. Chik, F. Md. Yassin, *J. Sci. Technol.* **2012**, *4*, 61.

[36] J. Isidorsson, C. G. Granqvist, K. von Rottkay, M. Rubin, *Appl. Opt.* **1998**, *37*, 7334.

[37] H. Wasa, K., Kanno, I., Kotera, *Handbook of Sputter Deposition Technology*, Elsevier Inc., **2012**.

[38] M. Navarro-Cía, S. A. Kuznetsov, M. Aznabet, M. Beruete, F. Falcone, M. Sorolla,

IEEE J. Quantum Electron. **2011**, *47*, 375.

[39] S. A. Kuznetsov, A. V. Arzhannikov, V. V. Kubarev, P. V. Kalinin, M. Sorolla, M. Navarro-Cía, M. Aznabet, M. Beruete, F. Falcone, Y. G. Goncharov, B. P. Gorshunov, A. V. Gelfand, N. I. Fedorinina, *Key Eng. Mater.* **2010**, *437*, 276.

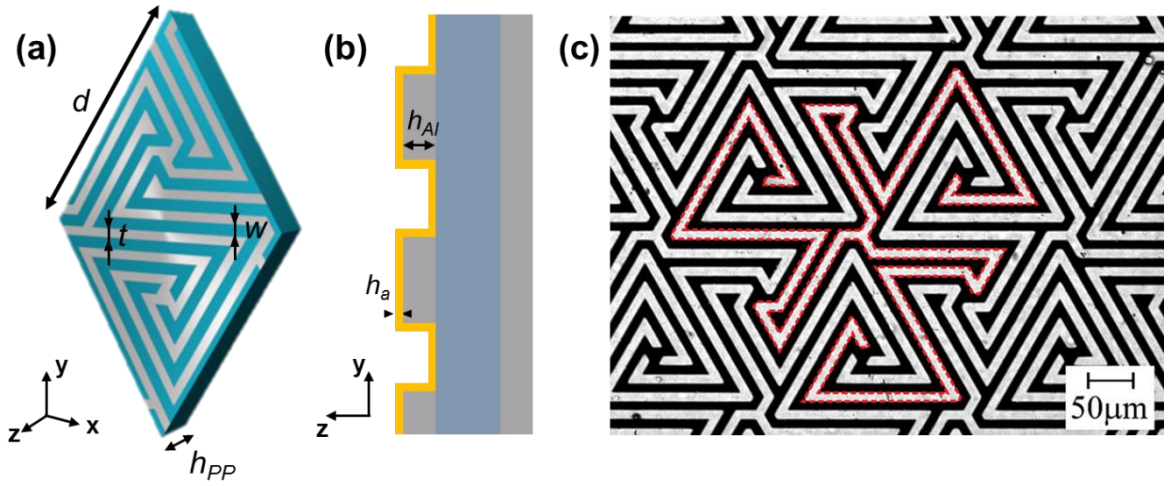

Figure 1. (a) Front view and (b) cross-section of the metasurface unit cell. In (a) the analyte has been omitted for clarity. Dimensions: d = 231 µm, h_{Al} = 0.4 µm, h_{PP} = 50 µm, t = 8.9 µm, w = 11.1 µm, h_a = 24 nm; 58 nm; 108 nm; 345 nm. Metallization is shown in grey. (c) Microscopic image of the labyrinth pattern on the PP substrate. The red dotted lines delimit the boundaries of the elementary convoluted-shape aperture used for creating a periodic metallic pattern of the metasurface.

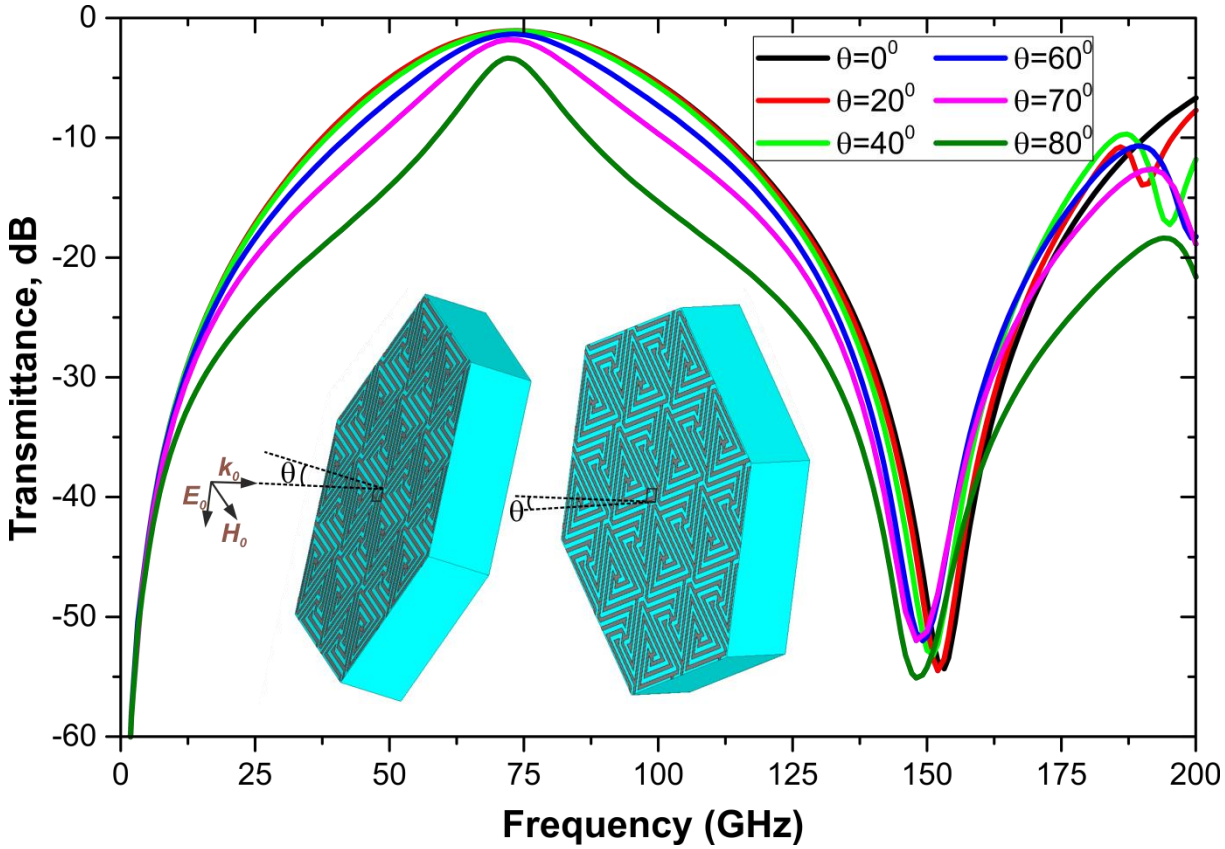

Figure 2. Simulated spectral transmittance of the GP-free 50um-PP-backed labyrinth metasurfaces in a bilayer multiplex (non-interference) configuration at different angles of incidence θ. To avoid inter-layer interference the indivual metasurfaces are inclined in mutually orthogonal planes with respect to the impinging wave. The resulted transmittance of such a bilayer structure is evaluated as a product of the single metasurface transmittances for TE- and TM-polarizations that is plotted here.

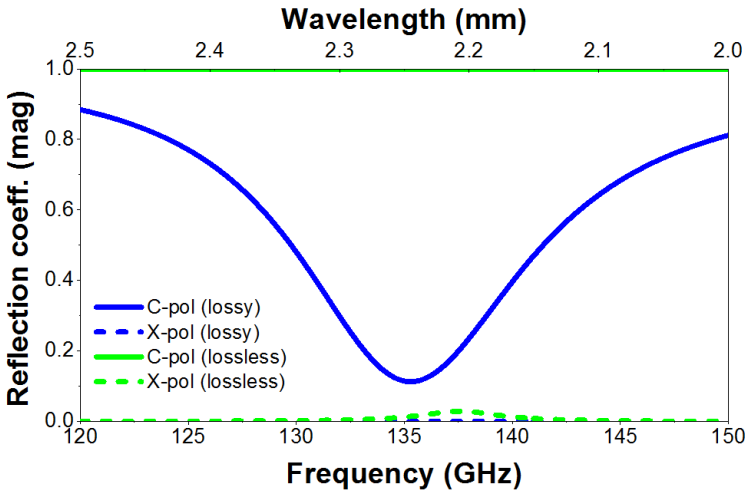

Figure 3. Reflection coefficient magnitude of the free-standing labyrinth metasurface absorber shown in Fig. 1. Lossless (green) and lossy (blue) scenarios are considered for both copolar (solid) and crosspolar (dashed) cases.

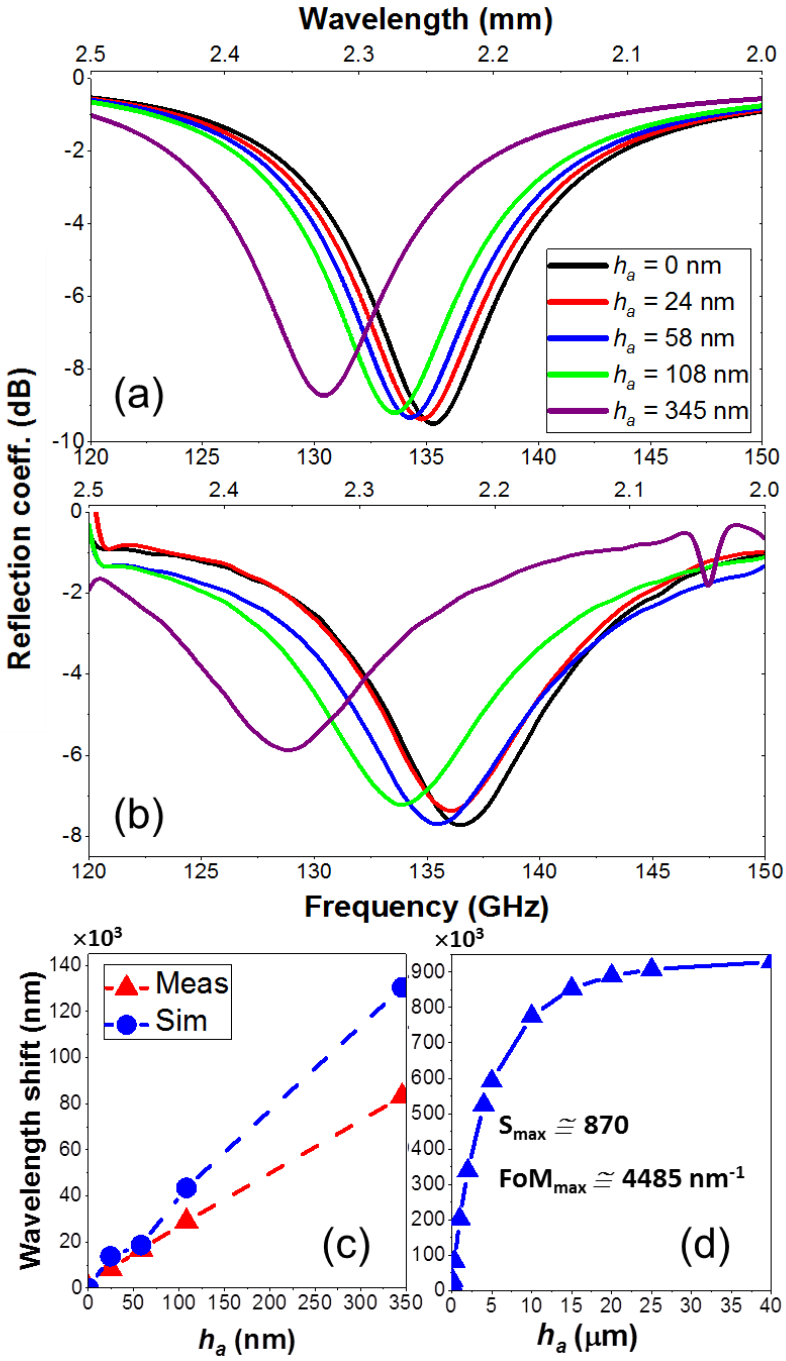

Figure 4. (a) Simulated and (b) experimentally measured spectra of the reflection coefficient for the labyrinth metasurface absorber under normal incidence and different analyte thicknesses. (c) Wavelength shift as a function of the analyte thickness for extremely thin analytes, simulation (blue) and measurements (red), calculated as $\Delta\lambda = \lambda_a - \lambda_0$, with λ_a the resonance wavelength at each h_a and λ_0 the resonance wavelength without the analyte. (d) Idem for more general analyte thicknesses, to show the saturation of the response (only simulation).

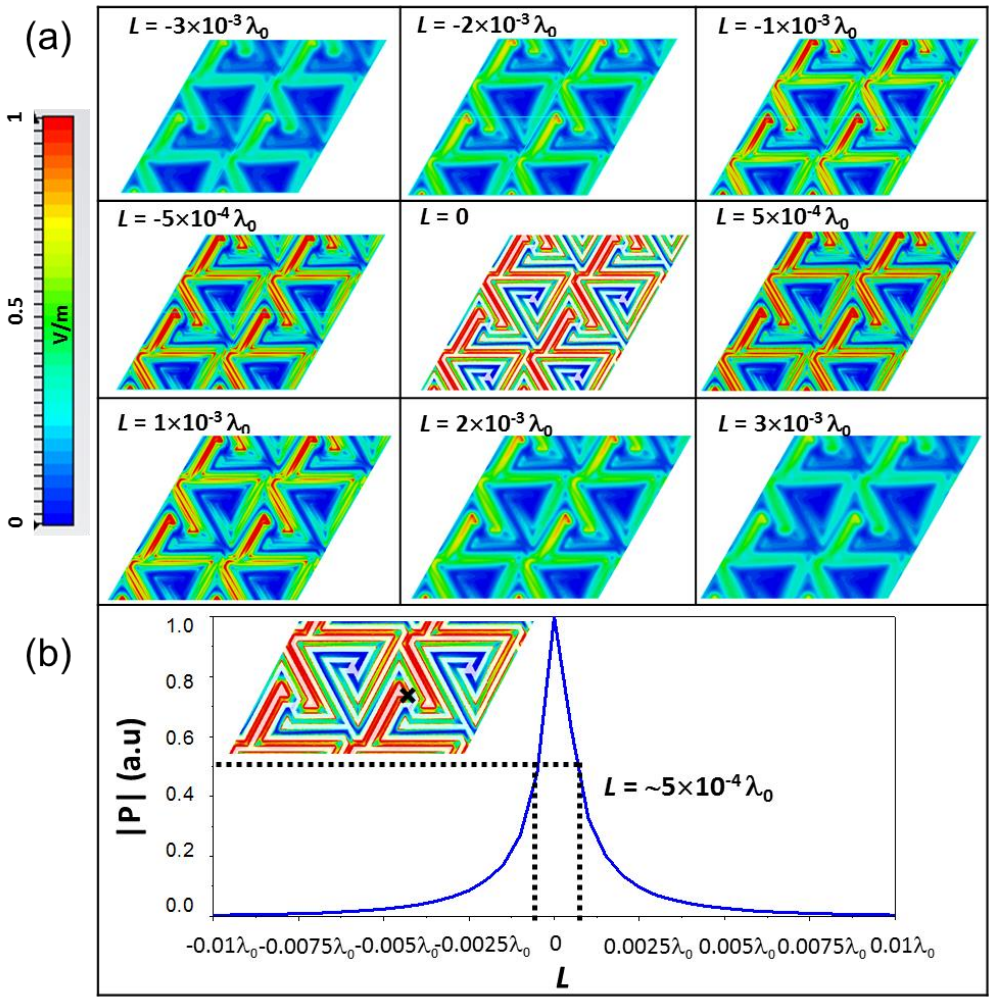

Figure 5. (a) Amplitude distribution of the electric field (absolute value) along the *z* axis at different distances (*L*, normalized to the operation wavelength) from the labyrinth metasurface absorber. (b) Normalized power vs distance at the point indicated by a cross in the inset.

Table 1. Sensitivity and FoM for each analyte thickness for the sample described in the main text calculated as $S = \Delta\lambda/h_a$ and FoM = S/FWHM. Both simulation (Sim) and experimental (Exp) values are presented.

h_a (nm)	Sensitivity		FoM [nm^{-1}]	
	Exp	Sim	Exp	Sim
24	346.67	569.07	2028.66	3613.28
58	498.3	552.47	3027.77	4297.43
108	578.07	870.77	3558.51	4485.84
345	349.98	549.27	2351.44	4131.40
Average value	443.25	635.39	2741.6	4181.98

Table 2. Sensitivity and FoM for each analyte thickness for the sample described in the supporting information calculated as $S = \Delta\lambda/h_a$ and FoM = S/FWHM. Both simulation (Sim) and experimental (Exp) values are presented.

h_a (nm)	Sensitivity		FoM [nm^{-1}]	
	Exp	**Sim**	**Exp**	**Sim**
100	306	321.1	2257.5	2344.9
150	247.6	315	1794	2332.1
200	243.4	300.1	1725.1	2198.6
Average value	265.7	312	1925.5	2291.9

Table 3. Comparison of different values of sensitivity and FoM achieved in different works, calculated as $S = \Delta\lambda/h_a$ and FoM = S/FWHM. FoM could not be obtained in some cases due to the impossibility of extracting the FWHM from the plots.

	Analyte Permittivity	Sensitivity (max.)	FoM (max) [nm^{-1}]
Ref. 20	2.56	4	-
Ref. 14	3.61	80	-
Ref. 15	2	3	118
This work	4	578	3558

((Supporting Information can be included here using this template))

Supporting Information

Labyrinth Metasurface Absorber for Ultra-High-Sensitivity Terahertz Thin Film Sensing

*Irati Jáuregui-López, Pablo Rodríguez-Ulibarri, Aitor Urrutia, Sergei A. Kuznetsov, Miguel Beruete**

I. Jáuregui-López, Dr. P. Rodríguez-Ulibarri, Dr. M. Beruete
Antennas Group-TERALAB
Electric and Electronic Engineering Department
Universidad Pública de Navarra
Campus Arrosadía, 31006 Pamplona, Spain
E-mail: miguel.beruete@unavarra.es

Dr. A. Urrutia, Dr. M. Beruete
Institute of Smart Cities
Public University of Navarra
31006 Pamplona, Spain

Dr. S. A. Kuznetsov
Novosibirsk State University
Pirogova 2, 630090 Novosibirsk, Russia.
Rzhanov Institute of Semiconductor Physics SB RAS
Novosibirsk Branch "TDIAM."
Lavrentiev Ave. 2/1, 630090 Novosibirsk, Russia
E-mail: SAKuznetsov@nsm.nsu.ru

Material and Methods

Fabrication of the metasurfaces

The metasurface was lithographically patterned over the area of 60 × 60 mm in a 0.4 μm thick aluminum (Al) layer sputtered on the PP film 50 μm thick via a vacuum thermal deposition method. Prior to sputtering, the PP film was treated with a glow discharge in argon atmosphere to improve adhesion of Al to PP. For patterning we employed a contact photolithography technique, which was specifically adapted to flexible solid film substrates, such as PP, whose industrial production does not allow obtaining a liquid phase suitable for posterior film deposition via spin coating[38,39]. After photolithography, a continuous aluminum layer 0.4 μm

thick was sputtered on an unpatterned side of the PP film to form the GP-layer of the metasurface. At the final fabrication stage the metasurface was tightened onto an annular Al holder with the clear aperture diameter of 50 mm matched to the experimental set-up used for spectral characterization.The metasurface dimensions were chosen from the condition of miniaturizing the electric size *d* of the metasurface unit cells taking into account the following output characteristics requirements and technological constraints:

- The widths of metallic lines t and inter-line gaps w in the metasurface pattern were required not to exceed the range of 10±2 μm.
- In a bilayer multiplex configuration the GP-free metasurface was obliged to possess a fundamental resonant pass-band centred at 75±3 GHz followed by a resonant stop-band centred at 150±3 GHz, which are to be stable upon changing the angle of incidence θ within the range of 0–80° (see the main text).

Analyte deposition and thickness characterization

The metasurfaces were pretreated with oxygen plasma and then coated with SnO_2 thin films by sputtering[37] using a DC-sputter coater (Quorum Emitech K675XD, from Quorum Technologies Ltd.) with a partial pressure of argon of 8×10^{-2} mbar and a current intensity of 90 mA. The SnO_2 target used was purchased from Plasmaterials, Inc. (99.9% purity). The deposition time was incrementally changed in order to fabricate thin films with different thicknesses. The thickness of the SnO2 thin films were measured experimentally with a profilometer (DektakXT, from Bruker).

Simulation set-up

All simulations in the paper were performed using the frequency domain solver of the full-wave commercial electromagnetic software CST Microwave Studio®. To model the structure as an infinite array, the regime of Floquet ports and unit cell boundary conditions applied to the designed unit cell was employed. A fine tetrahedral mesh with a minimum edge length of 54.47

nm was applied to resolve properly the details of the metallic labyrinth as well as the fine analyte layers. The aluminum part of the labyrinth pattern and the ground plane were modelled as a metal with an electric conductivity[27] $\sigma_{Al} = 1.5 \times 10^7$ S/m and thickness of 0.4 μm. The more than twofold conductivity reduction compared to bulky aluminum (3.6×10^7 S/m) is explained by the inherent surface roughness of PP films.[38] The PP substrate was modelled as a dielectric with the thickness $h_{PP} = 50$ μm and a complex dielectric permittivity with real part $\varepsilon = 2.25$ and delta tangent $\tan\delta \approx 1\times10^{-3}$, defined at the operation frequency $f_0 = 135.3$ GHz and fitted with a constant fit tangent delta function of order 2.[27,38] The SnO_2 analyte was modelled as a dielectric of variable thickness (from 24 nm to 350 nm) with a constant real permittivity $\varepsilon_a \cong 4$.

Experimental set-up

To carry out the experimental measurements an ABmm™ millimeter-wave vector network analyzer VNA equipped with a quasioptical bench was used. Measurements were performed in the D-band of the millimeter-wave spectrum that extends from 110 to 200 GHz. The principle of operation can be described as follows (see **Figure S1**): a vertically polarized pure Gaussian beam is transmitted by a corrugated horn antenna, with a beam radius of 12.9 mm. A pair of elliptical mirrors are placed in the beam path to collimate the beam at the location of the sample. Then, the beam is reflected back to the mentioned elliptical mirrors. In this work, the reflection configuration was employed, so that the source antenna also works as the receiver for the reflected signal. This is possible by using a directional coupler that steers the signal to the receiver. Before measuring the sample, it was necessary to calibrate the system. The calibration in the reflection configuration was done by removing the sample from the sample holder and placing a mirror instead. The sample was carefully placed at a proper phase plane by adjusting the *z* position with a precise micrometer screw.

Studying an alternative prototype

In order to prove the repeatability of our measurements, we performed a complete study of another labyrinth sample (sample II) by coating it with the SnO_2 analyte of dissimilar thicknesses than for the sample from the main text (sample I). Note, due to fabrication tolerance, the labyrinth pattern of the sample II had slightly different dimensions: t = 8.2 μm, w = 11.8 μm. **Figure S2** illustrates the sample's reflectivity for several thicknesses of the SnO_2 film ranging from h_a = 100 nm to h_a = 250 nm with a step of 50 nm. From the results shown in panels (a) and (b), one can trace a red shift for the reflectivity resonance when increasing the analyte thickness. The quantified values of this shift are displayed in panel (c). As reported in panel (d), the response saturates when the thickness approaches nearly 20 μm that repeats the result obtained with the sample I (see Figure 4(d) in the main text). In total, the experimental data plotted in Figure S2 and Figure 4 demonstrate good repeatability of the measurements.

Polarization characteristics

Susceptibility of the labyrinth metasurface absorber to the incident wave polarization was examined numerically via tracking the metasurface reflectance upon changing the E-field orientation angle for the linearly polarized wave. This study was accomplished by the example of the bare (analyte-free) sample II under normal excitation, as occurred in experiment. The polarization angle varied from 0° to 90° with an increment of 10°. As seen from the results presented in **Figure S3**, the metasurface spectrum remains unchanged at any polarization angle. That is an enormous advantage for sensing purposes.

Fractional losses

Regarding the absorption performance of the structure, it should be noticed that a bare PP substrate has low dielectric losses and is very thin in terms of wavelength ($\lambda_0/44$). The full-wave simulations show that in the absorber configuration this feature is kept: the energy is dissipated mainly via ohmic currents induced in the metallic layer of the labyrinth pattern. This

effect is illustrated in **Figure S4** where the fractional losses referred to the labyrinth pattern and the PP film are calculated as the functions of the normalized frequency, f/f_0.

Performance with lower permittivity

Note that in the studies that can be found in the literature, the analyte typically has a relatively low permittivity, in contrast with our study where $\varepsilon_a \cong 4$. To perform a fairer comparison with previous works, we did a simulation analysis using an analyte of lower permittivity: $\varepsilon = 2.56$ ($n = 1.6$). In **Figure S5(a)** is plotted the metasurface reflectivity as the analyte thickness varies from $h_a = 100$ nm to $h_a = 400$ nm, with a step of 50 nm. Derived from these results, the relative wavelength shift versus the analyte thickness is displayed in panel (b). We calculate the sensitivity and FoM following the same method of the main text ($S = \Delta\lambda/h_a$ and FoM = S/FWHM). With these numbers, we obtain the maximum sensitivity value of 184 and FoM of 1322 nm^{-1} for $h_a = 100$ nm.

Comparing sensitivity with alternative sensors

To perform a more detailed comparison between different works mentioned in the main text, we use two alternative sensitivity definitions of the sensor, as specified in Ref. 14 and Ref. 20 $S_1 = \Delta f(\%)/(n_a h_a)$, and $S_2 = \Delta f(\%)/h_a$. Here, $\Delta f(\%) = 100(f_a - f_0) / f_0$ with f_a the resonance frequency at each h_a and f_0 the resonance frequency without the analyte, $n_a = \sqrt{\varepsilon_a}$ is the analyte refractive index and h_a is the analyte thickness. With this definitions, it is possible to compare sensors of alternative designs operating in different spectral bands, and using analytes with varied electromagnetic properties. The results of sensitivity comparison are given in Table S1.

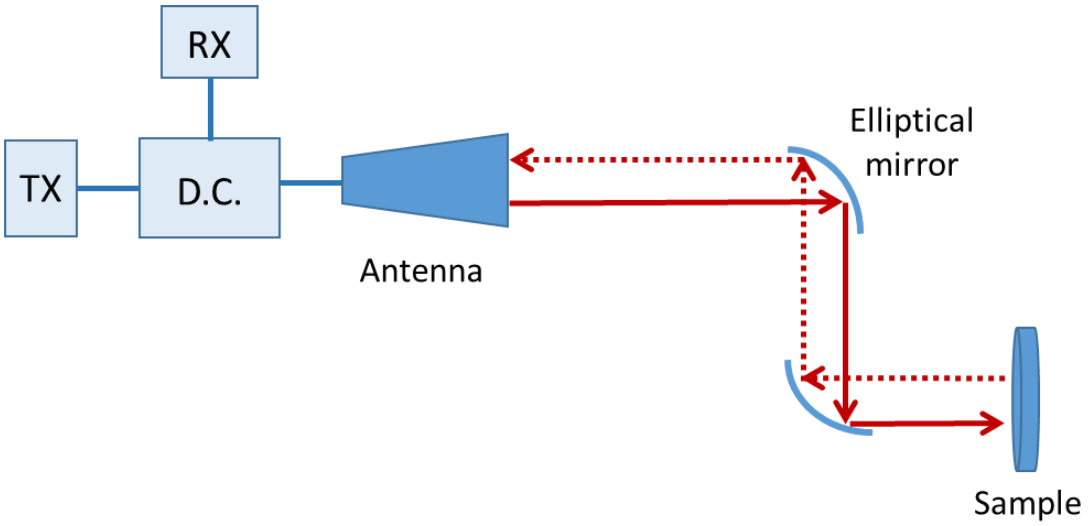

Figure S1. Schematic of the experimental set-up: The transmitter (TX) injects the power in the directional coupler (D.C.) and is then radiated by a corrugated horn antenna (Antenna). The radiated beam is steered and collimated onto the sample by a pair of elliptical mirrors. The reflected beam follows the same path and is collected by the antenna and steered to the receiver (RX) through the D.C. Red solid line: transmitted beam. Red dashed line: reflected beam.

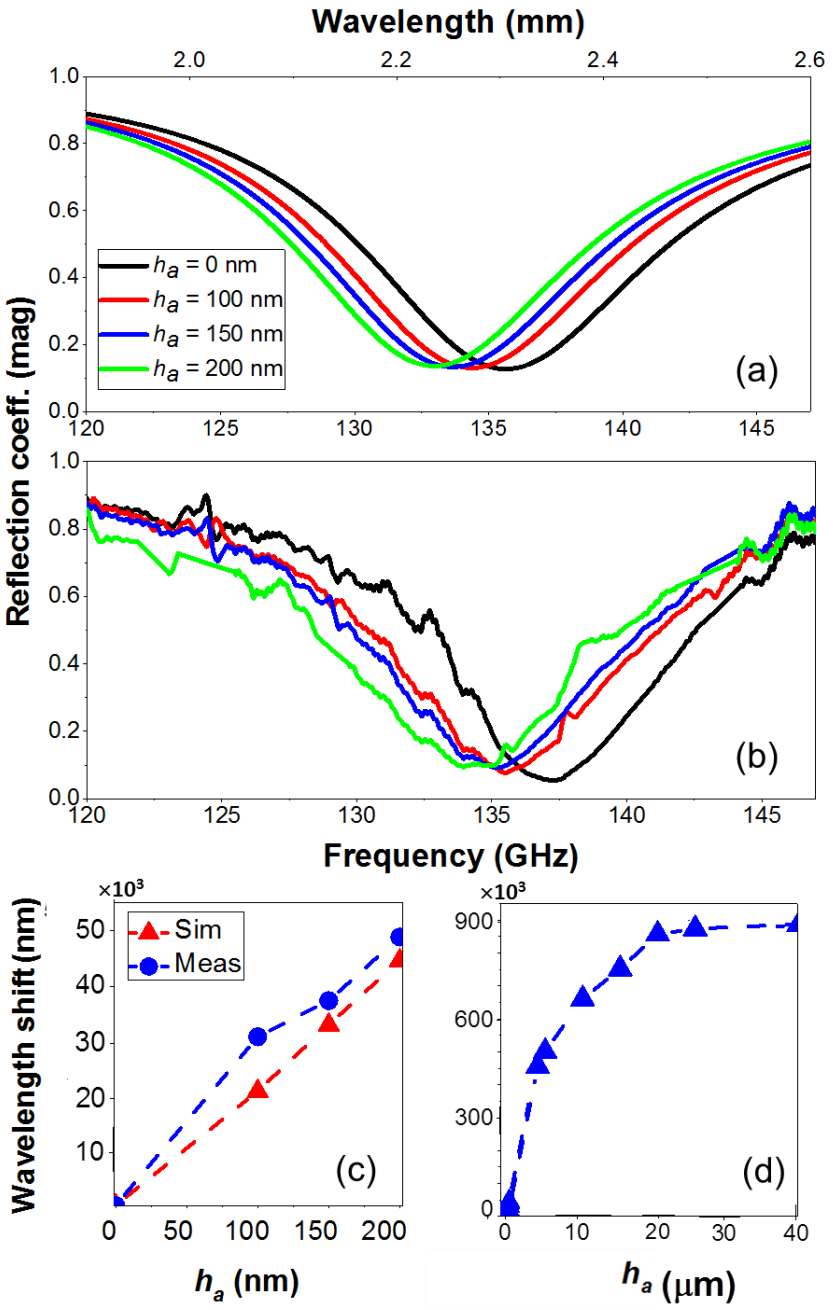

Figure S2. (a) Simulated and (b) experimentally measured spectra of the reflection coefficient for the labyrinth metasurface absorber under normal incidence at different analyte thicknesses. (c) Wavelength shift as a function of the analyte thickness for extremely thin analytes, simulation (blue) and measurements (red), calculated as $\Delta\lambda = \lambda_a - \lambda_0$, with λ_a the resonance wavelength at each h_a and λ_0 the resonance wavelength without the analyte. (d) Idem for more general analyte thicknesses, to show the saturation of the response (only simulation).

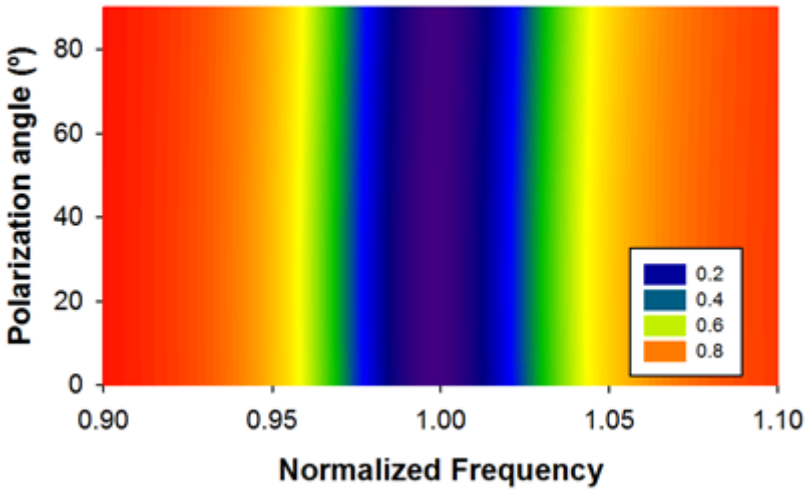

Figure S3. Referred to the normalized frequency f/f_0, spectral reflectivity of the labyrinth metasurface absorber plotted as a function of the polarization angle for the impinging wave. Linear scale, normal excitation.

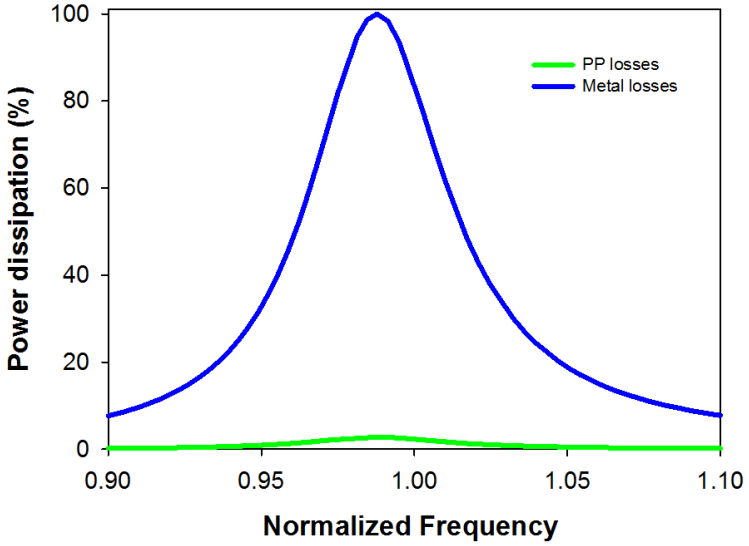

Figure S4. Fractional power dissipation (in %) vs the normalized frequency f/f_0 for the labyrinth metasurface absorber. Blue line: losses in metallization. Green line: losses in PP substrate.

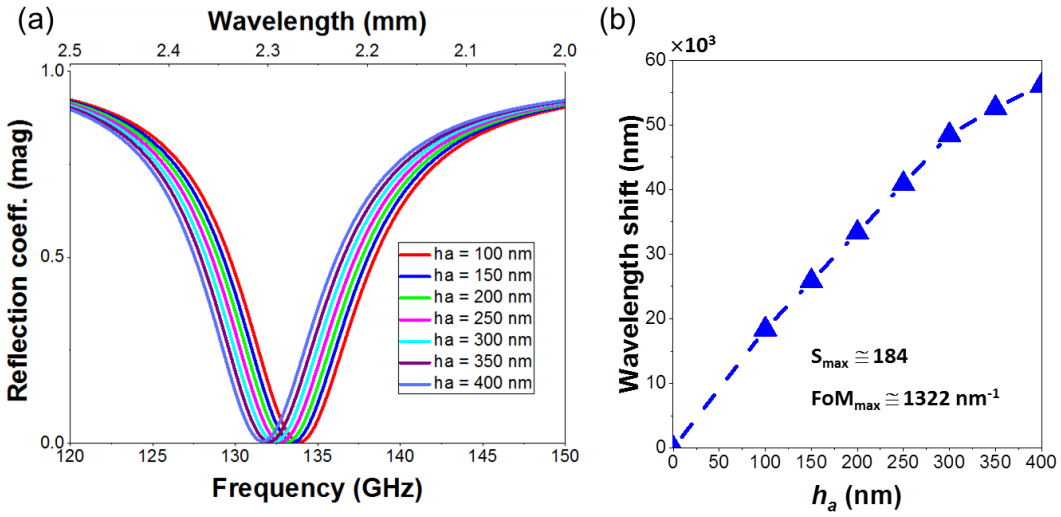

Figure S5. (a) Simulated reflection coefficient of the labyrinth metasurface absorber under normal incidence for an analyte with permittivity ε_a = 2.56 and different analyte thicknesses. (b) Wavelength shift as a function of the analyte thickness for extremely thin analytes, calculated as $\Delta\lambda = \lambda_a - \lambda_0$, with λ_a the resonance wavelength at each h_a and λ_0 the resonance wavelength without the analyte.

	Sensitivity #1 (max.) [%nm^{-1}]	Sensitivity #2 (max.) [%nm^{-1}]
Ref. 20 (main text)	5.07×10^{-4}	1.01×10^{-3}
Ref. 14 (main text)	6.76×10^{-3}	1.28×10^{-2}
Ref. 15 (main text)	3.88×10^{-4}	7.75×10^{-4}
This work	1.29×10^{-2}	1.76×10^{-2}

Table S1. Comparison for different values of sensitivity and in different works, where *S#1* = $\Delta f(\%)/\Delta n \cdot h_a$ [nm^{-1}], and *S#2* = $\Delta f(\%)/h_a$ [nm^{-1}].